Zeng *et al. Journal of Nanobiotechnology* (2025) 23:241
https://doi.org/10.1186/s12951-025-03319-9

Journal of Nanobiotechnology

RESEARCH Open Access

Recombinant human collagen hydrogels with different stem cell-derived exosomes encapsulation for wound treatment

Xiaoman Zeng[1,2], Jingjing Gan[2], Danqing Huang[2], Yuanjin Zhao[1,2,3*] and Lingyun Sun[1,2*]

Abstract

Exosomes-loaded hydrogels have potential value in wound treatment. Current studies focus on improving hydrogels' biocompatibility and optimizing different stem cell-derived exosomes for better therapeutic effect. Herein, we present a novel biocompatible recombinant human collagen (RHC) hydrogel loading with different MSCs-derived exosomes for promoting wound healing. We modify the RHC with methacrylate anhydride (MA) at optimal concentration, generating collagen hydrogel (RHCMA) with ideal physiochemical properties for exosome delivery (MSC-exos@RHCMA). Exosomes derived from human adipose-derived MSCs (ADSC-exos), bone marrow-derived MSCs (BMSC-exos) and umbilical cord MSCs (ucMSC-exos) are harvested from the culture supernatants and are loaded into RHCMA, respectively. These three hydrogel systems exhibit desired sustained release features, and can significantly improve cell proliferation and migration. In addition, these MSC-exos@RHCMAs show excellent therapeutic performance in treating the wounds of rats. Notably, we have demonstrated that the healing effect occurs best under the treatment of ucMSC-exos@RHCMA, following inflammatory resolution, angiogenesis, and collagen formation. These results would supply important value for the clinical application of MSC-exos in wound treatment in the future.

*Correspondence:
Yuanjin Zhao
yjzhao@seu.edu.cn
Lingyun Sun
lingyunsun@nju.edu.cn

Full list of author information is available at the end of the article

Graphical abstract

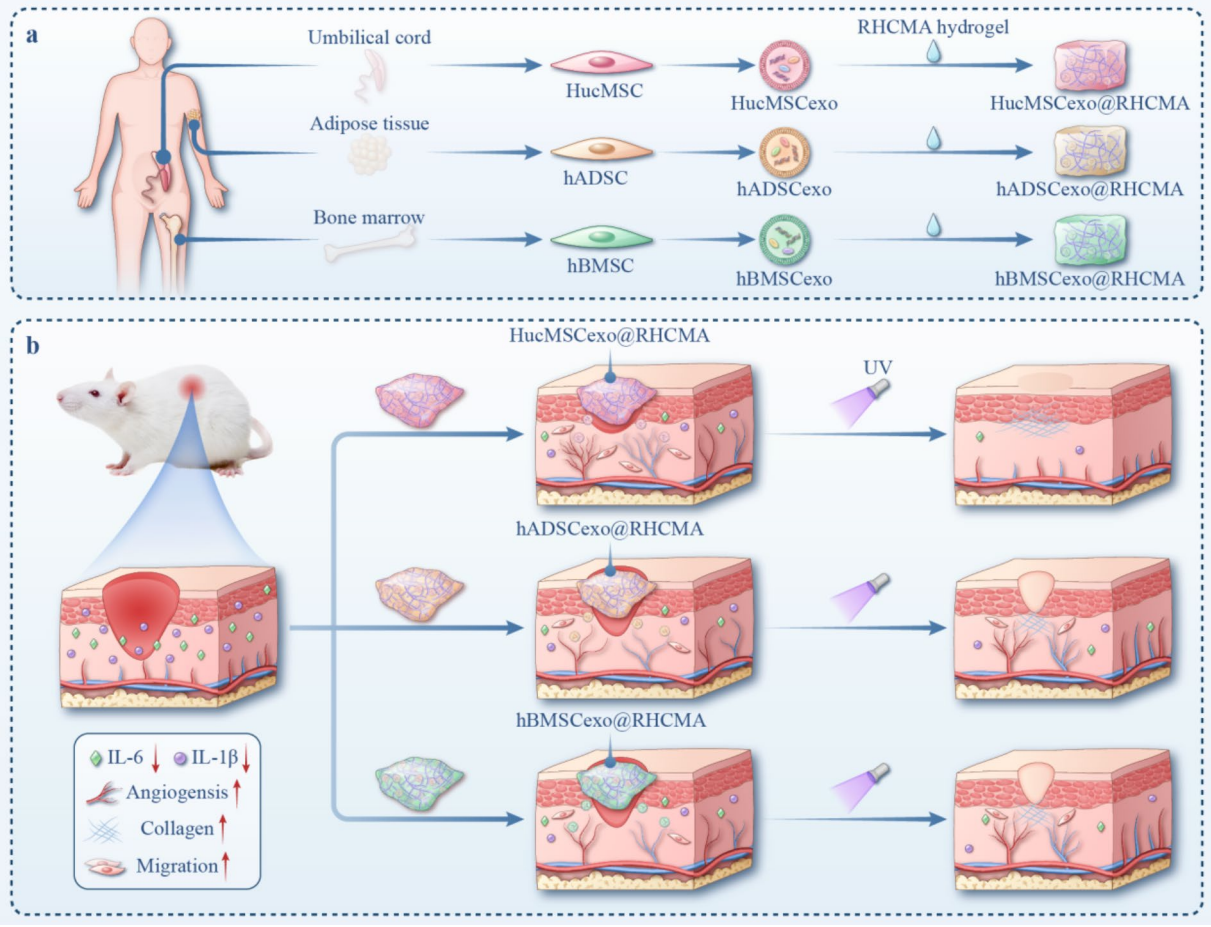

Keywords MSC, Exosome, Drug delivery, Wound healing, Hydrogel

Introduction

Delayed wound healing can be serious health threat and cause economic pressures for patients [1–6]. To date, various biological agents have emerged for accelerating wound closure and repair, such as mesenchymal stem cells (MSCs), recombinant proteins, exosomes, platelet-rich plasma and growth factors, etc [7–13]. Among them, MSC exosomes, as a class of MSC-derived extracellular vesicles within 40–160 nm, are rich as bioactive cargos of miRNAs, proteins, enzymes, and metabolites [14, 15]. With the release of these bioactive substances, exosomes can reduce inflammation, promote angiogenesis, accelerate cell proliferation and migration, showing great advantages in wound treatment [16]. MSC exosomes exhibit functional diversity depending on their cellular origin, reflecting the characteristics of their parent cells. In wound healing, exosomes derived from adipose-derived stem cells (ADSC-exos) primarily support blood vessel formation, while exosomes derived from bone marrow-derived MSCs (BMSC-exos) mainly boost cell growth and survival. Compared to BMSC-exos, human umbilical cord mesenchymal stem cell exosomes (ucMSC-exos) help regulate macrophages, reduce oxidative stress and inflammation, and accelerate wound healing [17, 18]. Especially, to maintain the exosomes' natural bioactivity and enhance their efficacy in wound healing, numerous biomimetic hydrogel scaffolds have been applied [19–23]. By encapsulating exosomes into hydrogels with biocompatibility and porous structures, exosomes can be enriched at wound site and be sustained released to improve the therapeutic efficacy [24–27]. However, due to the wide variety of stem cells, few reports have explored the comparative therapeutic effects of different cell-derived exosomes in wound treatment. In addition, most hydrogels applied for exosome encapsulation are synthetic and non-natural, remaining controversial regarding safety and immunogenicity [21, 28]. Thus, optimizing exosomes and hydrogels for improving wound treatment effect is still anticipated.

Herein, we proposed a novel human recombinant collagen hydrogel encapsulating exosomes derived from various stem cells to enhance wound healing, as schemed in Fig. 1. MSCs, known for their self-renewal and differentiation capabilities, are present virtually in all tissues, such as umbilical cord blood (UCB) [29], bone marrow [30], adipose tissue [31], and dental pulp [32]. Functions of these MSCs vary according to their species, so do the exosomes they secret. However, little attention has been given to investigating the detailed potential efficacy of different MSCs-derived exosomes for impaired wound repair. In contrast, various natural biomaterials have been utilized to carry exosomes because of their excellent biocompatibility and outstanding biodegradability [33, 34]. Among them, recombinant human collagen with methacrylate anhydride modification (RHCMA), as a human-derived hydrogel, is an attractive candidate for biomedical applications [35]. Owing to the ordered microstructures of recombinant human collagen (RHC), it can induce extracellular matrix remodeling and promote tissue regeneration, showing promising potential in wound treatment [36–38]. Therefore, a detailed comparative study on skin damage repair was performed using the combination of RHC and different stem cell-derived exosomes.

In this study, we synthesized RHCMA hydrogel by incorporating MA into the macromolecular chain of RHC by a condensation reaction [35]. As the physical properties and swelling behavior of the hydrogel could be precisely tuned by adjusting the RHCMA concentration, an optimal hydrogel system could be tailored for controlled drug release. Exosomes derived from human umbilical cord MSCs (ucMSCs), bone marrow-derived MSCs (BMSCs) and adipose-derived stem cells (ADSCs) were isolated via ultracentrifuge method [7, 20, 39], in which the purified ucMSC-exos, BMSC-exos, and ADSC-exos all possess clear membrane structures and uniform morphologies. By loading these three different MSC-derived exosomes into RHCMA hydrogel

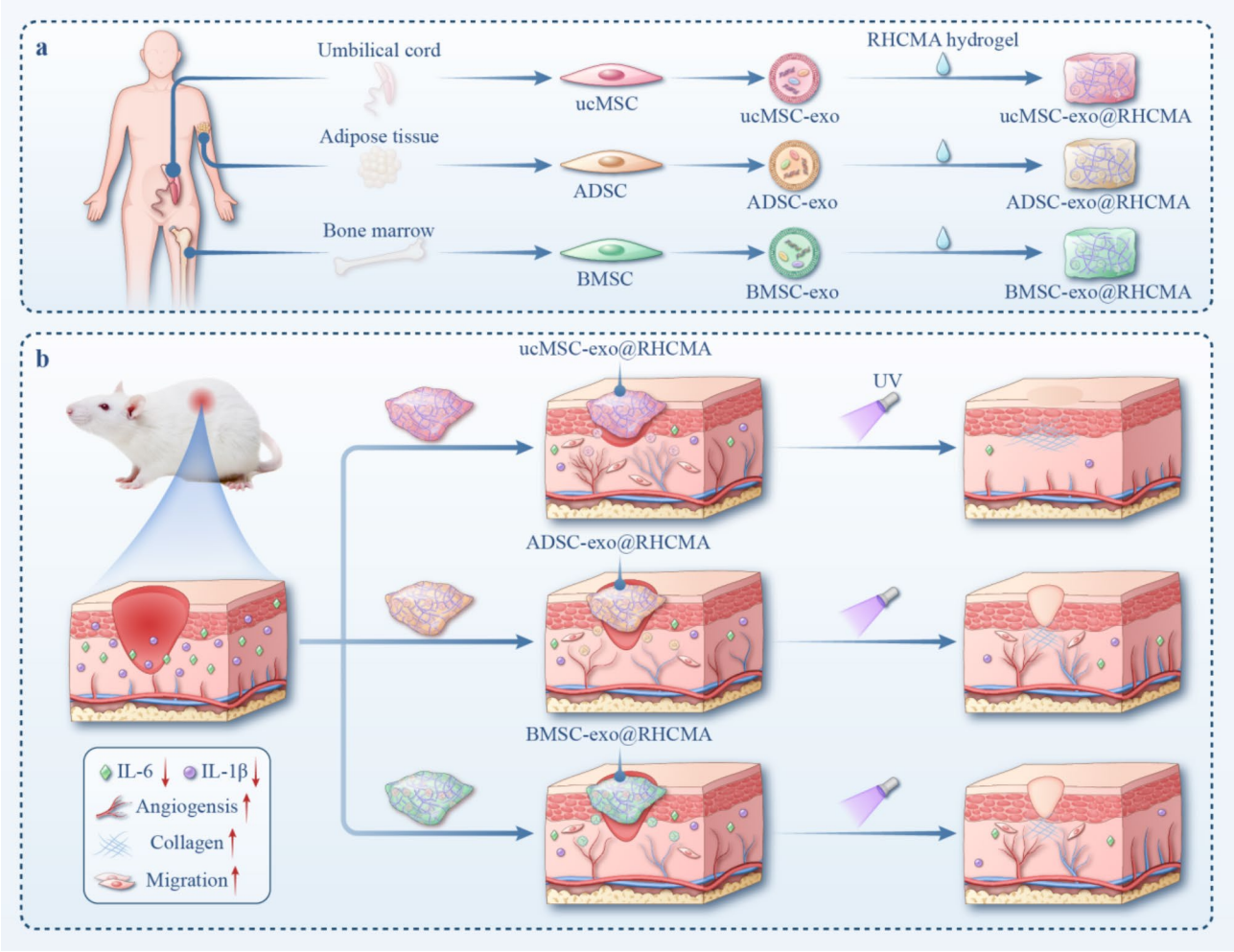

Fig. 1 (**a**) Schematic illustration of the preparation process of the three different MSC-derived exosome loaded RHCMA hydrogels; (**b**) Application of the hydrogels for promoting wound healing

respectively, we explored the in vitro effect of these sustained released-exosomes on cell migration, proliferation, and angiogenesis. In addition, we compared the therapeutic effects of these different exosomes-encapsulated RHCMA hydrogel in wound treatment on the skin defect rat model. It was found that among the three exosomes, the ucMSC-exos had better effect on accelerating wound healing by reducing inflammatory response, promoting angiogenesis and collagen deposition. Therefore, we believe that our study paves way for the future clinical application of MSC-derived exosomes in wound treatment.

Results and discussion

In our study, we aimed to enhance the collagen hydrogels' mechanical properties and preserve their excellent biocompatibility. We achieved this via chemically modify the collagen macromolecular chain with methacrylate anhydride (MA) and subsequently crosslinking it by a photoinitiator under UV light, we generated an RHCMA hydrogel for use in wound dressing, as illustrated in Fig. 2a. Characterization of RHCMA using ^{1}H NMR spectroscopy (Fig. S1a) revealed signals at 5.4 and 5.6 ppm, confirmed the presence of double bonds in the acrylic protons. Additionally, a peak at 1.8 ppm corresponding to methyl groups in methacrylate, thereby validating a successful synthesis of RHCMA. Fig. S1b presented visual images of 10% (w/v) RHCMA, both prior to and following gelation. To assess the influence of concentration on microstructure, mechanical strength, and swelling ratio, we further prepared 10%, 12.5%, 15%, and 17.5% w/v RHCMA pre-gel solutions. The structure of the hydrogel at varying densities were examined using scanning electron microscopy (SEM), as depicted in Fig. 2b-e. We confirmed that the size of micropores decreased with increased content of RHCMA pre-gels.

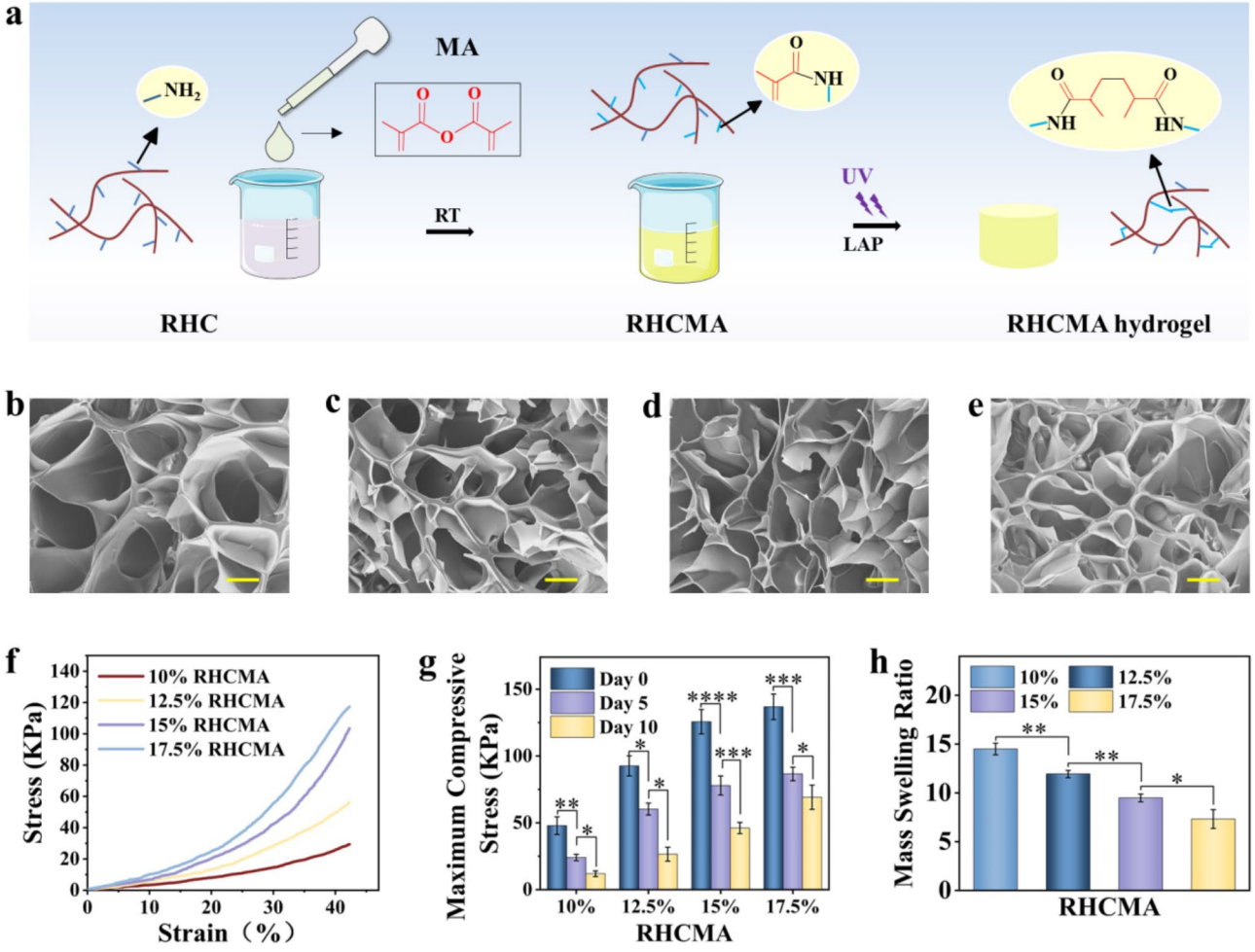

Fig. 2 Morphology and characteristics of RHCMA. (**a**) Schematic illustration of the synthesis of RHCMA hydrogels; (**b**-**e**) SEM images showing the porous structure of the RHCMA hydrogels at the concentration of 10%, 12.5%, 15%, and 17.5%, respectively. The scale bar is 50 μm; (**f**) Compressive strain–stress curves of the different RHCMA hydrogels after soaking in PBS for 60 min (day 0). (**g**) Histograms exhibiting the maximum compressive stress of the different RHCMA hydrogels after 0, 5, and 10 days of immersion in PBS ($n = 3$). (**h**) Histogram of the mass swelling ratio of the different RHCMA hydrogels ($n = 3$). *$p < 0.05$, **$p < 0.01$, ***$p < 0.001$, and ****$p < 0.0001$

Figure 2f-g described compressive strain-stress curves and maximum compressive stress of these hydrogels following immersed for 60 min (day 0), as well as after 5 and 10 days in phosphate buffer system (PBS). Analysis of the curves and histogram trends suggested that higher pre-gel concentrations notably enhance the mechanical properties of these hydrogels. For example, at day 0, the maximum compressive stress increased from 47.9 ± 6.6 kPa for a 10% concentration to 136.8 ± 9.6 kPa for a 17.5% concentration. The swelling ability of the hydrogels was investigated, as shown in Fig. 2h, increasing concentrations led to a reduced swelling ratio, from 14.5 ± 0.6 at 10% to 7.3 ± 1.0 at 17.5%. Besides, a test to investigate the mechanical properties of hydrogels and hydrogels incorporating with exosomes confirmed that there are no significant difference between the two (Fig. S2). This outcome was anticipated, as higher concentrations result in greater crosslinking density, consistent with previous findings [35]. Considering both mechanical strength and mass swelling, the physiochemical properties of the 10% RHCMA hydrogel closely similar to those of biological tissue [40].

Generally, hydrogel scaffolds for wound healing should be biocompatible, exhibiting low cytotoxicity and minimal inflammatory response when applied to injured skin. To assess the biocompatibility of these materials, the 3T3 cells were cultured with extracts from 10%, 12.5%, 15%, 17.5% RHCMA hydrogels and 10% RHCMA hydrogels loaded with three MSC exosomes, as well as from untreated group. The 3T3 cells revealed high viability with all constructs from live/dead staining results (Fig. 3a and b and S3, S4). The CCK-8 assay confirmed normal cell growth and proliferation on the RHCMA hydrogel surfaces, similar to cells cultured on cell culture plates (Fig. 3c and S5). Together, our results indicated that RHCMA had excellent biocompatibility, supporting their potential application as biomimetic scaffolds.

To study the performance of the RHCMA hydrogel as cargo delivery dressing, we investigated the in vitro release properties of ucMSC-exos from the hydrogels. Varying concentrations of RHCMA hydrogels (10%, 12.5%, 15%, and 17.5%) loaded with ucMSC-exos marked with fluorescent dye DID were immersed into PBS buffer over 3 days. The release kinetics of ucMSC-exos were presented in Fig. 3d. There was a noticeable increase in ucMSC-exos release from the 10% RHCMA patch, with 56.27 ± 4.48% released within the first 12 h. Subsequently, the release rate gradually decelerated, stabilizing after 48 h (92.27 ± 3.19%). During this process, no significant differences were observed in the release trends among RHCMA hydrogels with different concentrations. However, the 10% concentration exhibits a faster release rate. These results are likely due to the microporous structure of the RHCMA hydrogel. Consequently, the 10% RHCMA hydrogel was selected for use in all subsequent in vitro and in vivo experiments.

Stem cell exosomes, which exhibit therapeutic properties such as accelerating wound healing, are primarily derived from BMSCs, ADSCs, and ucMSCs. According to previous studies, exosomes were isolated and purified from the supernatants of BMSCs, ADSCs, and ucMSCs using ultracentrifuge method as previously described [7]. The morphologies of three MSC-derived exosomes were analyzed using transmission electron microscopy (TEM). As shown in Fig. 4a, they exhibited a bilayer vesicle structure resembling discoid, clear membrane integrity, uniform size distribution. Additionally, dynamic light scattering experiment indicated that the average size distribution of BMSC-exos, ADSC-exos, and ucMSC-exos were 102.6 ± 3.4 nm, 103.8 ± 3.3 nm, and 103.1 ± 3.8 nm, respectively (Fig. 4b and S6). This minor variation in diameter, which lacks statistical significance, is likely attributable to the diverse cargo encapsulated within the exosomes. Additionally, no significant differences were found in the zeta potential of three types of MSC-derived exosomes (Fig. S7). Western blot data confirmed the protein expression of exosome surface (TSG101 and CD63) (Fig. S8), verifying the proper exosome isolation. These data underscore the characteristics of exosomes sourced from BMSCs, ADSCs, and ucMSCs, affirming their suitability as unbound exosomes for subsequent experimental use.

Next, we evaluated the efficiency of ucMSC-exos uptake across various concentrations in human umbilical vein endothelial cells (HUVECs). As the dose of ucMSC-exos increased, there was a relevant enhancement in red fluorescence signal within the cytoplasm, reflecting enhanced intermembrane fusion events (Fig. 4c, f). Flow cytometry further confirmed that ucMSC-exosome uptake followed a time-dependent pattern (Fig. S9). Real-time quantitative PCR (RT-qPCR) analysis was performed to study the expression of cytokines in the samples. The expression levels of inflammatory cytokines, such as interleukin-1β (IL-1β) and interleukin-6 (IL-6), were significantly decreased in all three types of exosomes-loaded hydrogels (Fig. S10). Afterward, we examined the tube formation capability of HUVECs. Characteristic macroporous network structures were formed in all three MSC-exos@RHCMA treatment groups with a significantly higher number of tubular structures in the ucMSC-exos@RHCMA treatment group compared to the other two groups (Fig. 4d, g). Furthermore, the wound-scratch assay result also indicated that MSC-exos@RHCMA promoted endothelial cell migration in a co-culture system, with the MSC-exos@RHCMA groups migrating markedly faster than the control. The promoting trend among BMSC-exos@RHCMA, ADSC-exos@RHCMA, and ucMSC-exos@

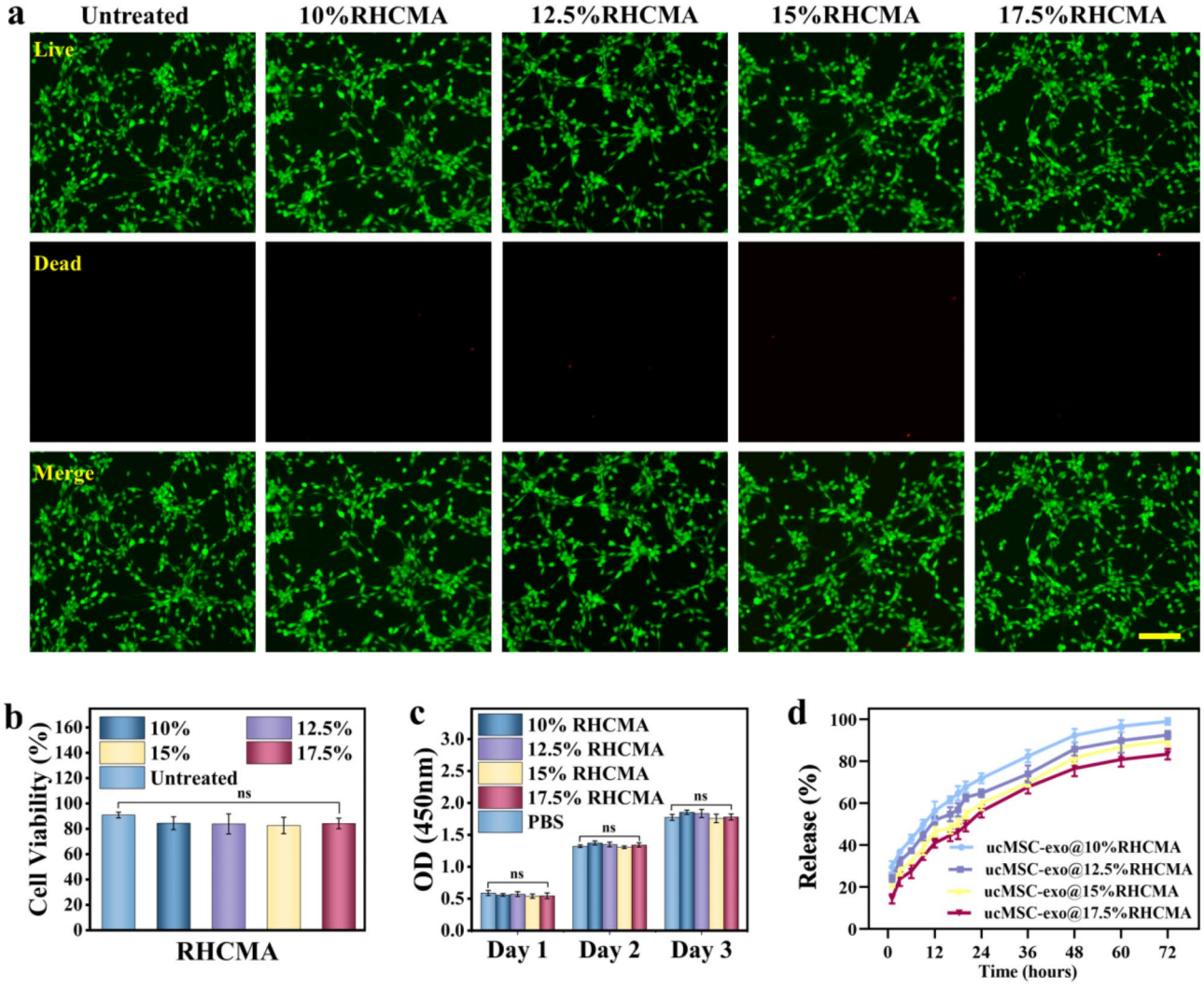

Fig. 3 In vitro cell viability and release of MSC-exos from RHCMA hydrogels. The Fibroblast cell line, 3T3, was used as the model cell line. (**a**) Confocal fluorescence images of 3T3 cells treated with different samples for 24 h, where Calcein AM and PI stained the cells, green represented live cells, and red showed dead cells. Cells were exposed to extracts from the untreated, 10% RHCMA, 12.5% RHCMA, 15% RHCMA, 17.5% RHCMA. The scale bar is 500 μm. (**b**) Histogram representing the statistical distribution of (a); $n = 5$; ns, no significant. (**c**) The cell growth of 3T3 cells on the RHCMA hydrogel with different concentrations over 3 days; $n = 5$; ns, no significant. (**d**) Corresponding release kinetics of MSC-exos from MSC-exo@10% RHCMA, MSC-exo@12.5% RHCMA, MSC-exo@15% RHCMA, and MSC-exo@17.5% RHCMA in PBS

RHCMA groups is increasing, with no significant differences observed (Fig. 4e, h).

Based on the above findings that RHCMA hydrogel can sustain release MSC-exos and that three MSC-exos@RHCMA could promote the endothelial cells migration and angiogenesis, we assess its potential in a rat wound model (Fig. 5a). The 1 cm-wounds on rats were categorized into five groups, receiving treatments of PBS, RHCMA hydrogel, BMSC-exos@RHCMA, ADSC-exos@RHCMA, and ucMSC-exos@RHCMA. Wounds in all animals were observed and photographed immediately after treatment, as well as at 5, 7, and 9 days post-operation, as shown in Fig. 5b. The ucMSC-exos@RHCMA treatment group demonstrated a significantly smaller wound area through the healing process, consistent with the quantitative data of wound pictures. Evaluation at various time points revealed that the ucMSC-exos@RHCMA group exhibited the fastest wound contraction compared to BMSC-exos@RHCMA, ADSC-exos@RHCMA, and RHCMA alone (Fig. 5d and e).

To elucidate the healing effects within wound beds, we performed a detailed histological analysis employing hematoxylin and eosin (H&E) and Masson's trichrome staining (Fig. 5g-h and S11). H&E staining revealed that wounds received three MSC-exos@RHCMA hydrogels showed accelerated repair processes and increased skin thickness compared to both the RHCMA and PBS groups (Fig. 5f). Notably, among the groups, the

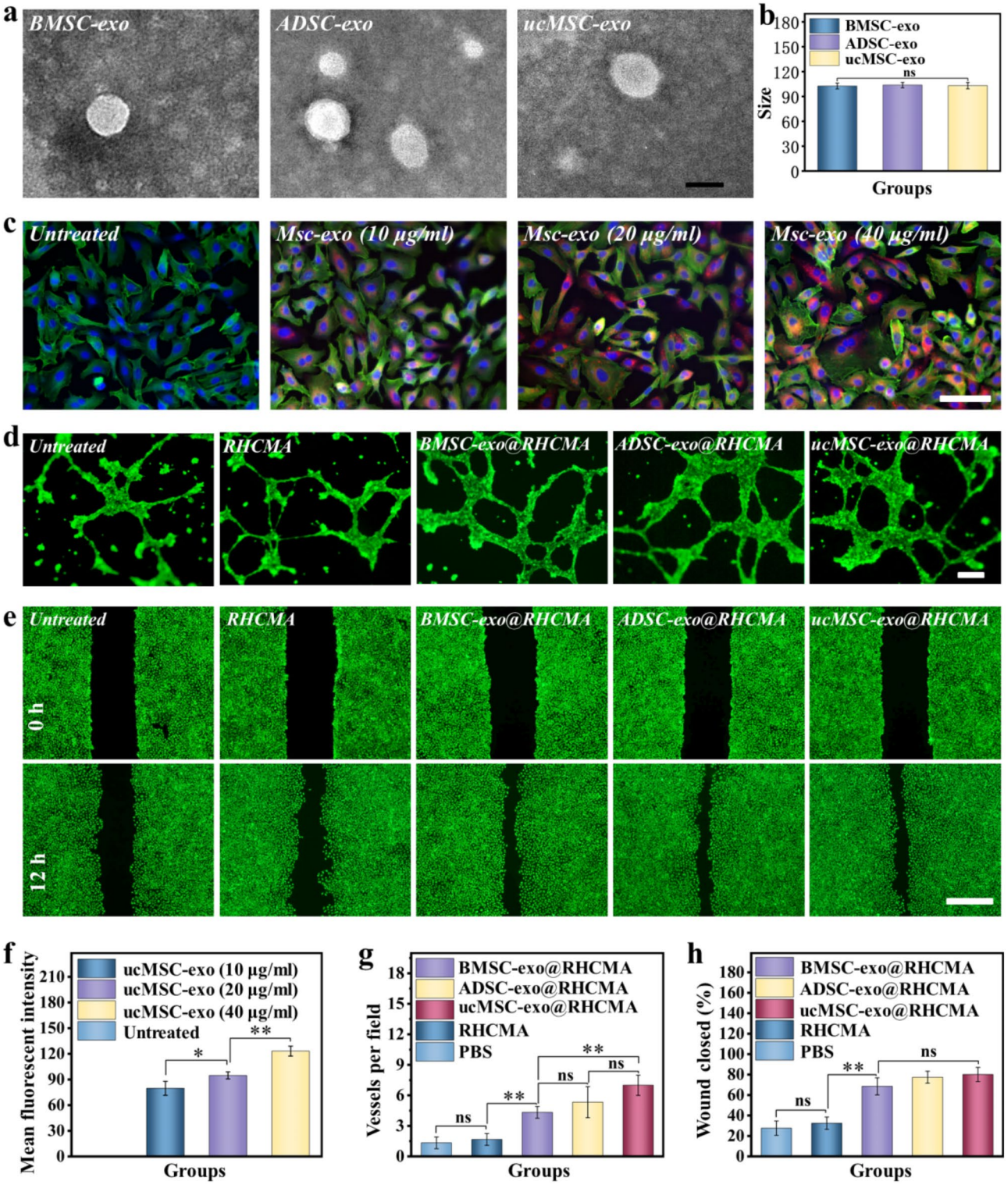

Fig. 4 (See legend on next page.)

(See figure on previous page.)

Fig. 4 Characteristics of the three MSC-exos and different MSC-exo@RHCMA promoted endothelial cell angiogenesis, migration in vitro. (**a**) Exosomes derived from BMSCs, ADSCs, and ucMSCs were visualized using TEM, scale bar is 100 nm. (**b**) Particle size distribution of MSC-exosomes determined using DLS. (**c**) HUVECs treated with different concentrations (10, 20, and 40 μg/mL) of DID-labeled MSC-exosomes or left untreated (PBS) for 6 h. Cellular uptake was assessed using confocal fluorescence microscopy, with scale bar indicating 100 μm. (**d**) Representative images of tube formation by HUVECs on matrigel after co-culture with BMSC-exos@RHCMA, ADSC-exos@RHCMA, and ucMSC-exos@RHCMA, compared to untreated conditions, for 12 h. Scale bar is 200 μm. (**e**) Representative images of scratch wound demonstrating the migration and repair capabilities of HUVECs when cultured with three different MSC-exos@RHCMA in comparison to control conditions. Scale bar is 400 μm. (**f**) Quantitative analysis of HUVECs uptake of DID-labeled MSC-exosomes, generating histograms to visualize the efficiency of exosome internalization ($n=5$). (**g**) Quantitative data of tube number per field ($n=3$). (**h**) Quantification of scratch test ($n=3$). $^{**}p<0.01$; ns, no significant

ucMSC-exos@RHCMA treated group exhibited the most coalesced skin. The regenerated collagen fibers appeared more aligned in the treated groups, indicating improved structural integrity and functionality of the healed tissue. The presence of adequate collagen deposition, a key indicator of effective wound healing, was further corroborated by Masson's trichrome staining, highlighting a marked increase in collagen density within the ucMSC-exos@RHCMA group relative to other groups (Fig. S12). This robust collagen deposition suggested enhanced tissue regeneration facilitated by ucMSC-exos@RHCMA, emphasizing its effectiveness in promoting wound healing. Moreover, comparisons between ucMSC-exos@RHCMA, BMSC-exos@RHCMA, ADSC-exos@RHCMA groups, and the RHCMA group illustrated the superior wound healing promotion capabilities of these treatments. Among the three exosomes, ucMSC-exos had best effect, with BMSC-exos and ADSC-exos showing similar efficacy. These findings validated MSC-exos@RHCMAs' therapeutic potential in enhancing wound healing outcomes, particularly in improving tissue regeneration and collagen alignment.

To further elucidate the mechanisms underlying wound repair facilitated by the three MSC-exos@RHCMA, wound tissues were assessed using immunofluorescence analysis of IL-1β, CD31 (an endothelial cell marker), and IL-6 after 9 days of treatment (Fig. 6a). As anticipated, the three MSC-exos@RHCMA treatment significantly down-regulated IL-1β expression in the wound beds post 9-day injury (Fig. 6b). Moreover, while minimal microvascular formation was observed in the control group, MSC-exos@RHCMA significantly promoted angiogenesis, evidenced by a substantial increase in blood vessel density. On day 9, CD31 levels were notably higher in the ucMSC-exos@RHCMA group compared to all other groups (Fig. 6c), consistent with the staining pictures. Additionally, IL-6 levels were notably reduced in the MSC-exos@RHCMA treatment groups (Fig. 6d). Quantitative analysis further showed a marked reduction in the IL-6-positive area in the ucMSC-exos@RHCMA, BMSC-exos@RHCMA, and ADSC-exos@RHCMA groups (Fig. 6d). These findings suggest that MSC-exos@RHCMA therapy promotes wound healing by attenuating pro-inflammatory cytokines like IL-1β and IL-6, and by enhancing angiogenesis, as evidenced by increased CD31-positive blood vessels. Besides, a complete blood panel on day 9 showed no statistical difference between RHCMA and PBS groups in immune response (Fig. S13), underscoring its potential utility as a biomimetic scaffold. Toxicity assessment of major organs via H&E staining (Fig. S14) confirmed the safety of the treatment material. Thus, our results demonstrate that the three MSC-exos@RHCMA accelerates wound healing through improved closure rates, angiogenesis, and collagen modulation. Among them, ucMSC-exo@RHCMA performed best.

Conclusion

In this study, we explored which types of MSC-exos is more effective for skin tissue repair and to develop the most biocompatible hydrogel scaffold as sustained release system. We isolated three kinds of MSC-exos and synthesized a novel recombinant human collagen hydrogel for wound treatment. We determined that a 10 wt% hydrogel concentration provided optimal mechanical properties and swelling characteristics similar to native structure. The efficacy of RHCMA hydrogel with different MSC-exos were demonstrated, showing that all three kinds of MSC-exos could accelerate cell proliferation, migration, and neovascularization in vitro. Among them, ucMSC-exo performed best, followed by ADSC-exo. The RHCMA hydrogel with MSC-exos promoted tissue repair by enhancing vascular reconstruction and collagen deposition, ultimately facilitating the regeneration of injured skin tissue in rat wound model. The ucMSC-exo exhibited superior therapeutic potential. These findings highlight the promising value of novel hydrogels with ucMSC-exos for tissue repair and regenerative medicine.

Experimental section

Materials

RHC was bought from Jiangsu JL and Biotech Corporation (China). The cell culture-related materials, including Dulbecco's modified Eagle's medium (DMEM), Fetal Bovine Serum (FBS), Penicillin-Streptomycin (PS), and trypsin were from Gibco (USA). Calcein AM (KGMP012-1) and propidium iodide (PI, KGA214) were obtained from KeyGEN BioTECH. The cell Live-Dead assay kit, CCK-8 were suplied by Thermo fisher (USA). IL-1β (Gb11113), IL-6 (Gb11117) and CD31 (Gb113151) antibodies were obtained from Servicebio technology Co.,

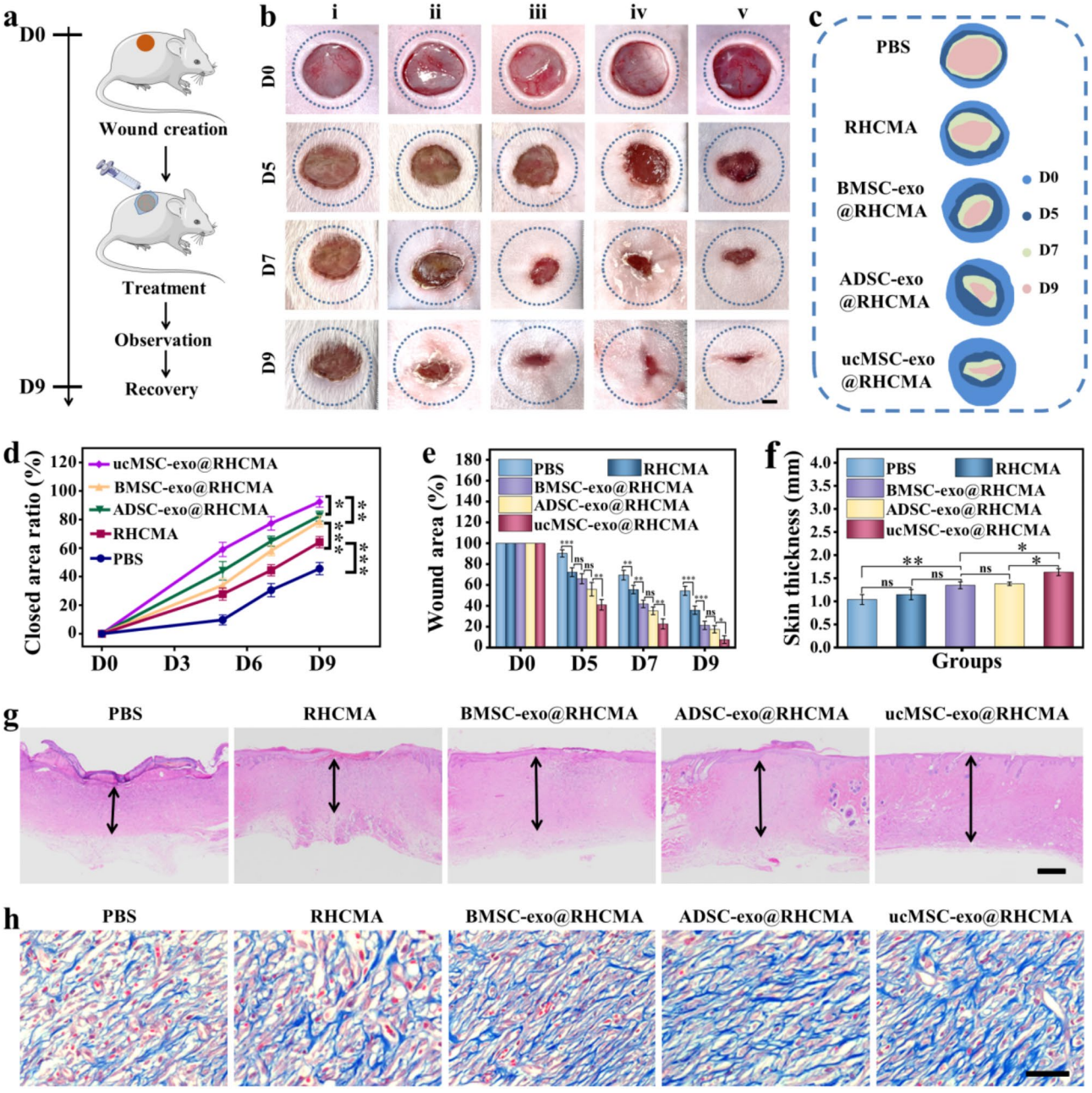

Fig. 5 In vivo wound healing evaluation of different MSC-exos@RHCMA. (**a**) Schematic description of animal experiments; (**b**) Representative optical images of wounds on day 0, 5, 7, and 9. i: PBS, ii: RHCMA, iii: BMSC-exos, iv: ADSC-exos, and v: ucMSC-exos. Scale bar, 3 mm. (**c**) Wound area tracing analysis corresponding to optical images shown in Fig. 5b. (**d**, **e**) Kinetics of wound closure ($n = 4$). (**f**) Statistical analysis of histological dermal thickness ($n = 4$). (**g**) H&E staining of wound tissue in different groups on day 9; the dermis is marked by segments; Scale bar is 500 μm. (**h**) Masson's trichrome staining of the wound tissue on day 9; scale bar is 50 μm. *$p < 0.05$, **$p < 0.01$, ***$p < 0.001$, and ****$p < 0.0001$; ns, no significant

Ltd. All chemical materials not mentioned were procured from Sigma-Aldrich (USA). 3T3 cells and HUVECs were provided by the Cell Bank (Shanghai). Six-week-old male Sprague–Dawley (SD) rat was sourced from the Model Animal Research Center of Nanjing University. Animal experiment received approval from the Animal Experiments Ethical Committee of Nanjing drum tower hospital.

Preparation of RHCMA

Freeze-dried human recombinant collagen was dissolved in DPBS (Hyclone) to achieve a 10% concentration, followed by stirring for 1 h at room temperature. Next, MA (2 mL) was incrementally added into 40 mL of this 10% collagen solution, with continuous stirring at 26 °C for an additional hour to promote methacrylation. The reaction was terminated by the introducing 30 mL of DPBS. After

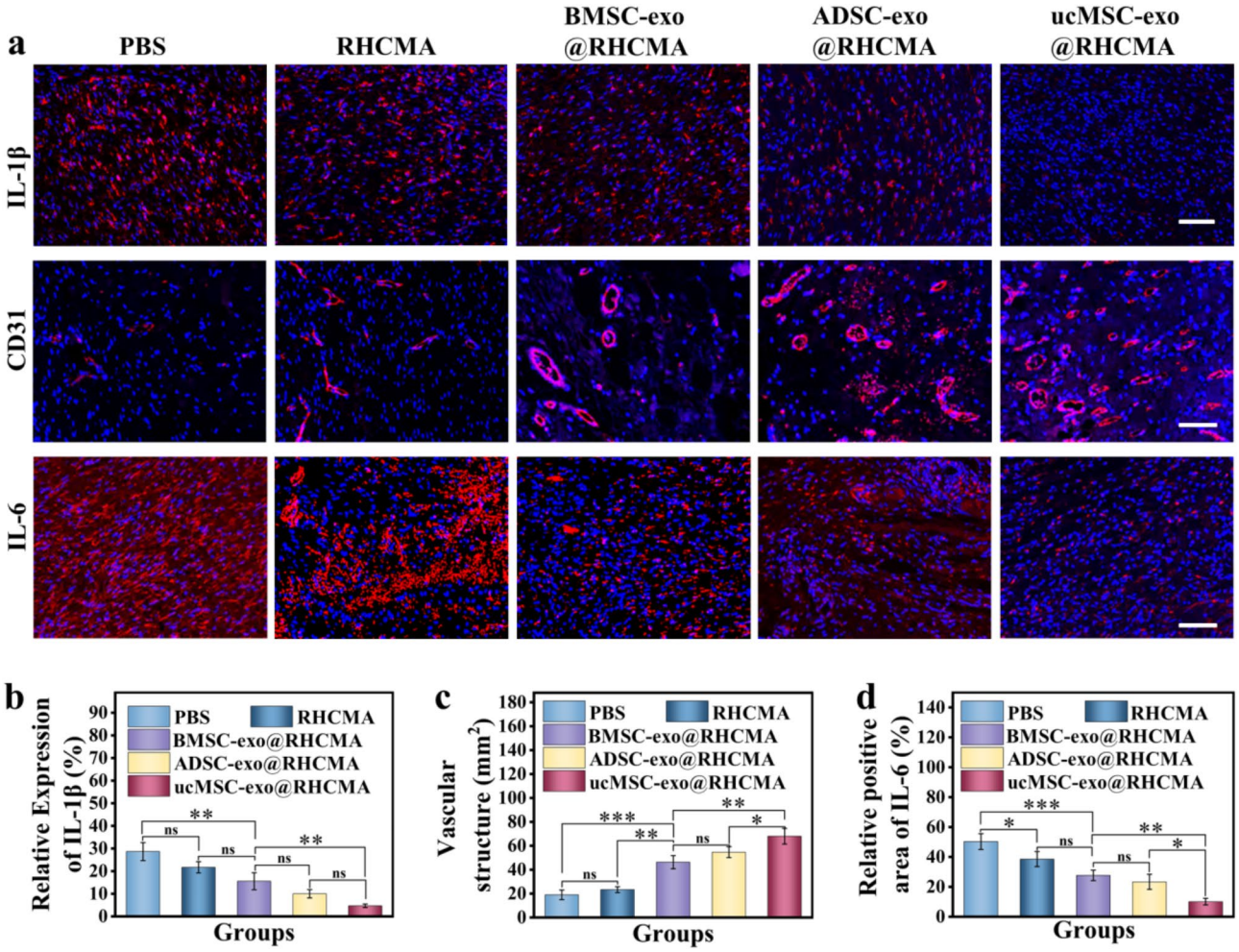

Fig. 6 Inflammatory cytokines were reduced and blood vessels increased in wound areas of rats with different MSC-exos@RHCMA treatment after 9 days. (**a**) Distribution of IL-6, HUVECs (CD31+) and IL-1β in the wound beds at 9 days after wounding. The scale bar, 100 μm. (**b**-**d**) Statistical analysis of (**b**) IL-1β, (**c**) CD31 + cells, and (**d**) IL-6 ($n = 4$). *$p < 0.05$, **$p < 0.01$, ***$p < 0.001$; ns, no significant

that, the resulting solution was dialyzed in deionized water for 5–7 days. At last, dialyzed solution was lyophilized to produce RHCMA sponge. RHCMA and the photoinitiator, lithium 2-hydroxy-2-methyl-1-phenylpropane (HMPP), were dissolved in DPBS and then photopolymerized under UV light for 60 s to prepare RHCMA hydrogels at different concentrations (10%, 12.5%, 15%, and 17.5%). To evaluate gelation properties, optical pictures of the hydrogel was captured, including those of the 10% RHCMA prior to and following gelation.

MSC-exos isolation and identification

MSCs were sourced from human adipose tissue, bone marrow, and umbilical cord, provided by the Stem Cell Center of Jiangsu Province. These MSCs were cultured at approximately 70% confluency. Next, they were transferred to exosome-depleted media and cultured for 48 h. The supernatants from these cultures were collected and subjected to ultracentrifugation to isolate exosomes. The resulting exosome pellets were resuspended in PBS and stored at -80 ℃ for further use. The freshly prepared exosome sample were observed using TEM. Size distribution and zeta potential was assessed using dynamic light scattering (Malvern).

Western blot analysis

MSCs and their purified exosomes of three distinct types were first diluted 1:4 with 5× protein loading buffer, then heated to 99.9 °C for approximately 6 min. The protein samples were separated using 10% SDS-PAGE, transferred to PVDF membranes. Following transfer, which were blocked with nonfat milk and then washed three times with TBST buffer, each wash lasting 10 min. The membranes were then incubated overnight at 4 °C with primary antibodies: rabbit anti-TSG101, mouse anti-CD63, and GAPDH for loading control. Detection was carried out using HRP-conjugated secondary antibodies

specific to either mouse or rabbit, protein bands were visualized with an Odyssey infrared imaging system.

MSC-exos loading and release

In our study, MSC-exos labeled with DID were employed. The preparation involved combining DID-labeled MSC-exos (1 mg/mL) with RHCMA solution, and photoinitiator, which was then placed into a cylindrical mold and subjected to ultraviolet light polymerization. Subsequently, the DID-labeled MSC-exos@RHCMA were submerged in PBS buffer at room temperature. At specified intervals—1, 3, 6, 9, 12, 18, 24, 36, 48, 60, and 72 h—the buffer was sampled, with an equal volume of fresh medium added. The release kinetics of the DID-labeled MSC-exos were tracked at each interval, with the initial content in the hydrogel set to 1.

Cell cultures and cellular uptake

3T3 and HUVEC cells were cultured in high-glucose DMEM supplemented with 10% fetal bovine serum. Cells were maintained in a 37 °C incubator with a 95% air and 5% CO2 atmosphere, and the culture medium was replaced every two days until the cells reached the desired confluence. For the assessment of cellular uptake, MSC-exos were labeled with DID (red, 1 mM). HUVECs were plated on 24-well glass plates and subsequently exposed to the DID-labeled MSC-exos at 10, 20, and 40 μg/mL concentrations. After incubation, these cells were washed with PBS and fixed with paraformaldehyde at room temperature for 10 min. The cytoskeleton was visualized using Phalloidin-iFluor 488, while cell nucleus was counterstained with DAPI for 10 min. Exosome uptake was assessed via confocal microscopy.

Cytotoxicity assessment

Cytotoxicity was evaluated using a live/dead staining kit. RHCMA extracts at concentrations of 10%, 12.5%, 15%, and 17.5% were prepared by immersing the materials in sterile PBS for 3 days. 3T3 cells, grown to approximately 70% confluence, were then exposed to these extracts, as well as to PBS as a control, in cell incubator for 24 h. The cell treatments included PBS, and RHCMA extracts at 10%, 12.5%, 15%, and 17.5% concentrations. After incubation, cells were stained with Calcein-AM and propidium iodide (PI) to assess cell viability. Fluorescence microscopy (Olympus) was used to visualize the staining patterns, and ImageJ software was utilized to quantify cell survival rates across the different treatment groups.

Cell proliferation evaluation with CCK-8 kit

Cell proliferation on hydrogels was assessed employing Cell Counting Kit-8 (CCK-8). Hydrogels, each with a diameter of 6.5 mm and a height of 1 mm, were fabricated using a custom mold and subsequently placed into a 96-well plate. 3T3 cells were seeded on either the hydrogel surfaces or standard cell culture plates ($n = 6$) and cultured for 1, 2, and 3 days. Following these periods, cells were exposed to CCK-8 solution for 2 h in cell incubator until the solution turned orange. Absorbance at 450 nm was then measured with a microplate reader to quantify the extent of cell proliferation, with the blank control subtracted. Each sample was tested in triplicate.

cDNA synthesis and quantitative RT-PCR analysis

Total RNA was extracted from the cells using the TRIzol reagent according to the manufacturer's protocol. The RNA concentration and purity were determined, and primers were designed using Primer Premier 5.0 software (sequences provided in Table 1). cDNA was synthesized using a One-Step RT-PCR kit following the manufacturer's instructions. GAPDH was used as an internal control gene. Quantitative PCR (qPCR) was performed on an ABI Vii7 real-time PCR system. The reaction conditions were as follows: 95 °C for 30 s (initial denaturation); 95 °C for 10 s (denaturation), 60 °C for 30 s (annealing), for 40 cycles; followed by a final extension at 72 °C for 10 min. Relative gene expression levels were calculated using the $2^{-\Delta\Delta CT}$ method.

Tube formation assay

To evaluate angiogenesis within a co-culture system, a tube formation assay was conducted [41]. Initially, 50 μL of Matrigel were dispensed into each well of a 96-well plate and allowed to solidify in a cell incubator for 30 min to allow gel solidification. Subsequently, 1×10^4 HUVECs were seeded on each well. After an initial medium aspiration, the wells were replenished with serum-free DMEM. Each well received treatments of PBS, RHCMA loaded with BMSC-exos, RHCMA loaded with ADSC-exos, or RHCMA loaded with ucMSC-exos. After 12 h of co-incubation, capillary-like tube formation was visualized and documented using an optical microscope.

Migration assay

To evaluate cellular migration, a wound scratch assay was employed as previously described [42, 43]. HUVECs were

Table 1 Primer Sequences for RT-qPCR Gene→Primer Sequence (5'–3')

No.	Gene name	Forward	Reverse
1	IL-1β	GAAATGCCACCTTTTGACAGTG	TGGATGCTCTCAT-CAGGACAG
2	IL-6	CATGTTCTCTGGGAAATCGTGG	AATGCCACCTTTT-GACAGTG
3	GAPDH	GGTGAAGGTCGGTGTGAACG	CTCGTCCCTG-GAAGATGGTG

Note: IL refers to interleukin, and GAPDH serves as the internal control for the PCR system

plated in six-well culture plates at a density of 1×10^5/mL and allowed to reach confluence. Following a 6-hour starvation period, a scratch was introduced into the cell monolayer using a 200 μL pipette tip. Subsequent to the removal of debris, these wells were replenished with fresh DMEM containing 0.25% FBS. Cells were treated with the specified conditions, and after 12 h of incubation, images of the HUVECs in each group were captured using a microscope equipped with a camera. The initial wound diameter was measured, and wound closure rates were quantified using ImageJ software.

In vivo therapeutic test

For the in vivo therapeutic evaluation, we established a full-thickness excisional wound model in Sprague-Dawley rats as previously described [44]. Under anesthesia, a 1 cm circular wound was created on the dorsal skin of each rat. After that, the rats were randomly divided into five groups of four each [45]. The first group was treated with PBS applied directly to the wound; the second group received RHCMA films placed on the wound beds; and the remaining three groups received the BMSC-exos@RHCMA, ADSC-exos@RHCMA and ucMSC-exos@RHCMA hydrogel, respectively. Each hydrogel dressing contains approximately 100 μg of exosomes. These hydrogels were instilled onto the wound beds and subjected to UV light for 60 s to achieve photopolymerization. Wounds were photographed on days 5, 7, and 9, with dressings replenished every 72 h. Wound healing was quantified using ImageJ software. On day 9, granulation tissues were harvested, sectioned, and evaluated using immunofluorescence staining (for IL-1β, CD31, and IL-6) and histological staining (H&E and Masson's trichrome). Additionally, major organs were harvested and analyzed histologically.

Statistical analysis

All experiments were performed in triplicate. Results are expressed as means ± standard error of the mean. Statistical comparisons between groups were made using Student's t-test, one-way ANOVA, and two-way ANOVA, analyzed with Origin 2019b software. Significance levels were set at $^{*}p < 0.05$, $^{**}p < 0.01$, $^{***}p < 0.001$, and $^{****}p < 0.0001$. Non-significant results are denoted as ns.

Supplementary Information

The online version contains supplementary material available at https://doi.org/10.1186/s12951-025-03319-9.

Supplementary Material 1

Acknowledgements
NA.

Author contributions
Y.J.Z. conceived the idea and designed the experiment; L.Y.S. provided funding support. X.M.Z. and J.J.G. conducted experiments, data analysis and wrote the manuscript; D.Q.H. assited with cell culture, revised the paper, and checked the data. All authors reviewed the manuscript.

Funding
This work was supported by the National Key Research and Development Program of China (2020YFA0908200 and 2020YFA0710800), the Key Program of the National Natural Science Foundation of China (81930043 and 82330055), the Joint Fund of the National Natural Science Foundation of China (U24A20380), the Nanjing Medical Science and Technique Development Foundation (ZKX21019).and the Clinical Trials from Nanjing Drum Tower Hospital (2022-LCYI-ZD-01).

Data availability
No datasets were generated or analysed during the current study.

Declarations

Ethics approval and consent to participate
All animal experiments were conducted in accordance with the principles and were approved by the Animal Experiments Ethical Committee of Nanjing drum tower hospital (No. 2021AE02007).

Consent for publication
All authors agree to submit for publication in "Journal of Nanobiotechnology".

Competing interests
The authors declare no competing interests.

Author details
[1]Department of Rheumatology and Immunology, Nanjing Drum Tower Hospital, School of Medicine, Southeast University, Nanjing, China
[2]Department of Rheumatology and Immunology, Nanjing Drum Tower Hospital, Medical School, Nanjing University, Nanjing 210002, China
[3]State Key Laboratory of Bioelectronics, School of Biological Science and Medical Engineering, Southeast University, Nanjing 210096, China

Received: 24 October 2024 / Accepted: 11 March 2025
Published online: 24 March 2025

References

1. Falanga V, Isseroff RR, Soulika AM, Romanelli M, Margolis D, Kapp S, Granick M, Harding K. Chronic wounds. Nat Rev Dis Primers. 2022;8:50.
2. Willenborg S, Eming SA. Cellular networks in wound healing. Science. 2018;362:891–2.
3. Wang L, Ding X, Fan L, Filppula AM, Li Q, Zhang H, Zhao Y, Shang L. Self-Healing dynamic hydrogel microparticles with structural color for wound management. Nanomicro Lett. 2024;16:232.
4. Yao X, Zhu G, Zhu P, Ma J, Chen W, Liu Z, Kong T. Omniphobic ZIF-8@Hydrogel membrane by Microfluidic-Emulsion-Templating method for wound healing. Adv Funct Mater. 2020;30:1909389.
5. Liu Y, Zhao X, Zhao C, Zhang H, Zhao Y. Responsive porous microcarriers with controllable oxygen delivery for wound healing. Small. 2019;15:e1901254.
6. Mao J, Chen L, Cai Z, Qian S, Liu Z, Zhao B, Zhang Y, Sun X, Cui W. Advanced biomaterials for regulating polarization of macrophages in wound healing. Adv Funct Mater. 2022;32:2111003.
7. Fang S, Xu C, Zhang Y, Xue C, Yang C, Bi H, Qian X, Wu M, Ji K, Zhao Y, et al. Umbilical Cord-Derived mesenchymal stem Cell-Derived Exosomal MicroRNAs suppress myofibroblast differentiation by inhibiting the transforming growth Factor-β/SMAD2 pathway during wound healing. Stem Cells Translational Med. 2016;5:1425–39.
8. Ebrahimian TG, Pouzoulet F, Squiban C, Buard V, André M, Cousin B, Gourmelon P, Benderitter M, Casteilla L, Tamarat R. Cell therapy based on adipose Tissue-Derived stromal cells promotes physiological and pathological wound healing. Arterioscler Thromb Vasc Biol. 2009;29:503–10.

9. Zhang B, Wang M, Gong A, Zhang X, Wu X, Zhu Y, Shi H, Wu L, Zhu W, Qian H, Xu W. HucMSC-Exosome Mediated-Wnt4 signaling is required for cutaneous wound healing. Stem Cells. 2015;33:2158–68.
10. Qi S, Zhang P, Ma M, Yao M, Wu J, Mäkilä E, Salonen J, Ruskoaho H, Xu Y, Santos HA, Zhang H. Cellular Internalization-Induced aggregation of porous silicon nanoparticles for ultrasound imaging and Protein-Mediated protection of stem cells. Small. 2019;15:e1804332.
11. Gurtner GC, Werner S, Barrandon Y, Longaker MT. Wound repair and regeneration. Nature. 2008;453:314–21.
12. Zhu H, Wu X, Liu R, Zhao Y, Sun L. ECM-Inspired Hydrogels with ADSCs Encapsulation for Rheumatoid Arthritis Treatment. Advanced Science, n/a:2206253.
13. Shan J, Che J, Song C, Zhao Y. Emerging antibacterial nanozymes for wound healing. Smart Med. 2023;2:e20220025.
14. Kalluri R, LeBleu VS. The biology, function, and biomedical applications of exosomes. Science. 2020;367.
15. Wiklander OPB, Brennan M, Lötvall J, Breakefield XO. El andaloussi S: advances in therapeutic applications of extracellular vesicles. Sci Transl Med. 2019;11.
16. Gan J, Zhang X, Ma W, Zhao Y, Sun L. Antibacterial, adhesive, and MSC exosomes encapsulated microneedles with spatio-temporal variation functions for diabetic wound healing. Nano Today. 2022;47:101630.
17. Li Y, Zhu Z, Li S, Xie X, Qin L, Zhang Q, Yang Y, Wang T, Zhang Y. Exosomes: compositions, biogenesis, and mechanisms in diabetic wound healing. J Nanobiotechnol. 2024;22:398.
18. Barlow S, Brooke G, Chatterjee K, Price G, Pelekanos R, Rossetti T, Doody M, Venter D, Pain S, Gilshenan K, Atkinson K. Comparison of human placenta- and bone marrow-derived multipotent mesenchymal stem cells. Stem Cells Dev. 2008;17:1095–107.
19. Lin J, Wang Z, Huang J, Tang S, Saiding Q, Zhu Q, Cui W. Microenvironment-Protected Exosome-Hydrogel for facilitating endometrial regeneration, fertility restoration, and live birth of offspring. Small. 2021;17.
20. Deng D, Li X, Zhang J-J, Yin Y, Tian Y, Gan D, Wu R, Wang J, Tian B-M, Chen F-M, He X-T. Biotin–Avidin System-Based delivery enhances the therapeutic performance of MSC-Derived exosomes. ACS Nano. 2023;17:8530–50.
21. Hu H, Dong L, Bu Z, Shen Y, Luo J, Zhang H, Zhao S, Lv F, Liu Z. miR-23a-3p-abundant small extracellular vesicles released from Gelma/nanoclay hydrogel for cartilage regeneration. J Extracell Vesicles. 2020;9:1778883.
22. Zhang H, Chen G, Yu Y, Guo J, Tan Q, Zhao Y. Microfluidic printing of slippery textiles for medical drainage around wounds. Adv Sci (Weinh). 2020;7:2000789.
23. Guo J, Yu Y, Zhang D, Zhang H, Zhao Y. Morphological Hydrogel Microfibers with MXene Encapsulation for Electronic Skin. Research (Wash D C) 2021;2021:7065907.
24. Yang L, Li W, Zhao Y, Shang L. Magnetic polysaccharide mesenchymal stem cells exosomes delivery microcarriers for synergistic therapy of osteoarthritis. ACS Nano. 2024;18:20101–10.
25. Wang Y, Guo J, Cao X, Zhao Y. Developing conductive hydrogels for biomedical applications. Smart Med. 2024;3:e20230023.
26. Lin X, Cai L, Cao X, Zhao Y. Stimuli-responsive silk fibroin for on-demand drug delivery. Smart Med. 2023;2:e20220019.
27. Chen G, Wang F, Zhang X, Shang Y, Zhao Y. Living microecological hydrogels for wound healing. Sci Adv. 2023;9:eadg3478.
28. Pezzana C, Cras A, Simelière F, Guesdon R, Desgres M, Correa BL, Peuffier A, Bellamy V, Gouarderes S, Alberdi A, et al. Biomaterial-embedded extracellular vesicles improve recovery of the dysfunctional myocardium. Biomaterials. 2022;291:121877.
29. Wang HS, Hung SC, Peng ST, Huang CC, Wei HM, Guo YJ, Fu YS, Lai MC, Chen CC. Mesenchymal stem cells in the Wharton's jelly of the human umbilical cord. Stem Cells. 2004;22:1330–7.
30. Bianco P, Gehron Robey P. Marrow stromal stem cells. J Clin Invest. 2000;105:1663–8.
31. Gronthos S, Franklin DM, Leddy HA, Robey PG, Storms RW, Gimble JM. Surface protein characterization of human adipose tissue-derived stromal cells. J Cell Physiol. 2001;189:54–63.
32. Gronthos S, Mankani M, Brahim J, Robey PG, Shi S. Postnatal human dental pulp stem cells (DPSCs) in vitro and in vivo. Proc Natl Acad Sci U S A. 2000;97:13625–30.
33. Xin L, Lin X, Zhou F, Li C, Wang X, Yu H, Pan Y, Fei H, Ma L, Zhang S. A scaffold laden with mesenchymal stem cell-derived exosomes for promoting endometrium regeneration and fertility restoration through macrophage Immunomodulation. Acta Biomater. 2020;113:252–66.
34. Yang L, Li W, Zhao Y, Wang Y, Shang L. Stem cell recruitment polypeptide hydrogel microcarriers with exosome delivery for osteoarthritis treatment. J Nanobiotechnol. 2024;22.
35. Kong B, Sun L, Liu R, Chen Y, Shang Y, Tan H, Zhao Y, Sun L. Recombinant human collagen hydrogels with hierarchically ordered microstructures for corneal stroma regeneration. Chem Eng J. 2022;428:131012.
36. Yang M, Chu L, Zhuang Y, Qi C, Meng S, Liu Z, Kong T. Multi-Material digital light processing (DLP) Bioprinting of heterogeneous hydrogel constructs with perfusable networks. Adv Funct Mater. 2024;34:2316456.
37. Kong B, Liu R, Hu X, Li M, Zhou X, Zhao Y, Kong T. Cornea-Inspired Ultrasound-Responsive adhesive hydrogel patches for keratitis treatment. Adv Funct Mater. 2023;34.
38. Zhu Y, Kong B, Liu R, Zhao Y. Developing biomedical engineering technologies for reproductive medicine. Smart Med. 2022;1:e20220006.
39. Théry C, Amigorena S, Raposo G, Clayton A. Isolation and characterization of exosomes from cell culture supernatants and biological fluids. Curr Protoc Cell Biol 2006; Chap. 3:Unit 3.22.
40. Kong B, Chen Y, Liu R, Liu X, Liu C, Shao Z, Xiong L, Liu X, Sun W, Mi S. Fiber reinforced GelMA hydrogel to induce the regeneration of corneal stroma. Nat Commun. 2020;11.
41. Huang D, Cheng Y, Chen G, Zhao Y. 3D-Printed Janus piezoelectric patches for sonodynamic bacteria elimination and wound healing. Research. 2023;6.
42. Wang X, Yang C, Yu Y, Zhao Y. In Situ 3D Bioprinting Living Photosynthetic Scaffolds for Autotrophic Wound Healing. Research 2022;2022.
43. Zhou X, Zhou Q, He Z, Xiao Y, Liu Y, Huang Z, Sun Y, Wang J, Zhao Z, Liu X, et al. ROS balance autoregulating Core–Shell CeO2@ZIF-8/Au nanoplatform for wound repair. Nano-Micro Lett. 2024;16:156.
44. Chi J, Sun L, Cai L, Fan L, Shao C, Shang L, Zhao Y. Chinese herb microneedle patch for wound healing. Bioactive Mater. 2021;6:3507–14.
45. Wang X, Yang C, Yu Y, Zhao Y. In Situ 3D Bioprinting Living Photosynthetic Scaffolds for Autotrophic Wound Healing. Research (Wash D C) 2022;2022:9794745.

Publisher's note